Resonant Excitation of Confined Excitons in Nanocrystal Quantum Dots Using Surface Plasmon-Polaritons

Yuliy V. Bludov* and Mikhail I. Vasilevskiy

Centro de Física, Universidade do Minho, Campus de Gualtar, Braga 4710-057, Portugal

E-mail: bludov@fisica.uminho.pt

KEYWORDS: surface plasmon-polariton; quantum dot; attenuated total reflection; superlattice

*To whom correspondence should be addressed

Abstract

Surface plasmon-polaritons (SPPs) in a multilayer structure consisting of a metallic film and one or more layers of nanocrystal (NC) quantum dots (QDs) are studied theoretically. It is shown that there is a resonance coupling between the plasmon-polaritons propagating along the metal/NC-layer interface and excitons confined in the dots, which produces a considerable effect on the optical properties of the structure unless the dispersion of the QD size is too large. Using a transfer matrix formalism, multilayer structures consisting of NC composite and metallic films are considered and it is demonstrated that the coupling extends over several layers constituting the structure. It can be explored in order to selectively excite QDs of different size by making a layer-by layer assembled NC planar structure and using an attenuated total reflection (ATR) configuration for the SPP-enhanced excitation of the dots. In particular, it opens the possibility to control the relative intensity of light of different color, emitted by the QDs of different size.

Introduction

Semiconductor quantum dots (QDs), often referred to as "artificial atoms", have discrete energy levels that can be tuned by changing the QD size and shape. The existence of zero-dimensional states in QDs has been proved by high spectrally and spatially resolved photoluminescence (PL) spectroscopy.[1,2] During the last decade, efforts have been concentrated on the studies of single QDs,[3] on one hand, and the development of new nanostructures using QDs as building blocks or combining them with traditional materials,[4,5] on the other hand. In the limit of large numbers of QDs, colloidal semiconductor nanocrystals (NCs) provide a promising route towards large-scale nanoassemblies.[5,6] With such artificial materials, exploiting the tunable optical properties of QDs, a number of devices such as light emitting diodes,[7] photodetectors[8] and photovoltaic cells[9] have been demonstrated.

In QD assemblies, the question of coupling and coherence between the dots naturally arises. Unlike single atoms, no two QDs are exactly the same and the energy levels fluctuate from dot

to dot. If these fluctuations are large, no collective excitations should be possible. Even though electronic excitations can, in principle, delocalize over multiple dots with a sufficiently uniform size, it requires a considerable probability of electron tunneling across the interface and a high degree of structural order in the QD assembly, conditions that are difficult to achieve.[6] In fact, electrical conductivity of ensembles of nanocrystal QDs is low, thermal-activated and probably mediated by a thermal-assisted hopping mechanism.[10] However, coupling between QDs can occur through a long-range electromagnetic interaction leading to the processes of energy transfer without charge transport. It requires resonance between the optical transitions in different QDs that can be separated by distances much larger than their size. Such processes have been proposed as mechanisms for the formation of extended coherent exciton states in regular arrays (superstructures) of QDs,[11,12] unidirectional energy transfer in size-gradient layered NC assemblies[6,13] and PL up-conversion in diluted QD ensembles.[14]

Colloidal chemistry techniques have proved the ability to synthesize high quality NCs with very uniform size, which can be varied in the range of 2–10 nm.[5] The size uniformity is important for the electromagnetic coupling between QDs. With these NCs, a broad variety of nanostructures can be prepared, in particular, multilayer structures of QDs of different average size, deposited on different substrates.[5] Combining such structures with other materials, such as organic dielectrics,[15] epitaxial quantum well heterostructures,[16] patterned metallic surface,[17,18] graphene,[19] or even biological molecules,[20] can result in new interesting physics and applications related to the energy transfer from photoexcited NCs to these materials or *vice versa*.

Recent experiments[21] demonstrated the possibility of strong coupling between excitons confined in NC quantum dots and surface plasmon-polaritons (SPPs) propagating along the interface of a silver film and the QD layer deposited on top of it. The observation was achieved by measuring attenuated total reflection (ATR) spectra of the structure. In this work we develop the theory of the observed effect taking into account the QD size dispersion. We will show that the resonant SPP coupling to excitons confined in QDs can be considerable unless the dispersion of the QD size is too large or the dots are too far from the metal/dielectric interface. The resonant coupling can be

used for controllable pumping the dots in order to explore their incomparable luminescence properties.[5] Based on the calculated results, we will discuss possible applications of the ATR structures containing, beyond the silver film, several layers of NCs of different average size.

The paper is organized as follows. First, we introduce the complex dielectric function for a composite medium containing semiconductor NCs and exemplify it for the case of CdSe QDs embedded in PMMA. Next, we obtain and illustrate the SPP dispersion relations and, finally, present and discuss the calculated results for the reflectivity of ATR structures containing several QD and metallic layers arranged in a number of different ways.

Dielectric function of a composite material containing quantum dots

A single QD can be described by a bare electronic susceptibility that takes into account inter-band transitions [1]:

$$\chi(\omega) = \frac{4\left|d_{cv}\right|^2}{3V}\sum_n \left[\frac{\left|\beta_n\right|^2}{E_n - i\Gamma - \hbar\omega} + \frac{\left|\beta_n\right|^2}{E_n - i\Gamma + \hbar\omega}\right], \tag{1}$$

where the sum runs over confined exciton states with energies E_i ($i = 0$ denotes exciton vacuum), d_{cv} is the transition dipole moment matrix element between valence and conduction bands of the underlying semiconductor material, V is the QD volume and

$$\beta_i = g_i \int_{QD} \Psi_{ex}^{(i)}(\mathbf{r},\mathbf{r})\, d\mathbf{r}$$

with g_i and $\Psi_{ex}^{(i)}(\mathbf{r}_e,\mathbf{r}_h)$ denoting the degeneracy factor and the wavefunction of the corresponding exciton states.

The quantity

$$\varepsilon_{QD}(\omega) = \varepsilon_s^{\infty} + 4\pi\chi(\omega) \tag{2}$$

[1] It relates the QD polarization to the electric field inside the dot.

can be regarded as a QD dielectric function, where ε_s^∞ is the high-frequency dielectric constant of the QD material. However, it can be more convenient to define the QD polarizability (assuming spherical shape of the dot),

$$\alpha(\omega) = \frac{\varepsilon_{QD}(\omega) - \varepsilon_h}{\varepsilon_{QD}(\omega) + 2\varepsilon_h} a^3 \,, \tag{3}$$

where a is the QD radius and ε_h is the dielectric constant of the host material. Using these quantities (2,3), one can calculate an effective dielectric function, ε^*, of the composite material containing uniform size QDs embedded in the host matrix using one of the following schemes:

(i) Maxwell-Garnett approximation (MGA) valid in the low QD concentration limit,[22]

$$\frac{\varepsilon^* - \varepsilon_h}{\varepsilon^* + 2\varepsilon_h} = \frac{4\pi}{3} N\alpha \,, \tag{4}$$

where N is the number of particles per unit volume;

(ii) Bruggemann mean field approximation (BA),[23]

$$f\frac{\varepsilon_{QD} - \varepsilon^*}{\varepsilon_{QD} + 2\varepsilon^*} + (1-f)\frac{\varepsilon_h - \varepsilon^*}{\varepsilon_h + 2\varepsilon^*} = 0 \,, \tag{5}$$

where $f = \frac{4\pi}{3} N a^3$ is the volume fraction of QDs. BA is valid when $f \sim 0.5$. MGA can be extended up to $f \sim 0.1$ using a renormalized polarizability which takes into account the dipole-dipole interactions between QDs as explained in Ref.[24]

The modified MGA (MMGA) proposed in Refs.[24,25] allows for taking into account the QD radius dispersion. Let $F(a)$ denote the radius distribution function. The renormalized polarizability, $\alpha^\star$, can be calculated by the following equations,

$$\alpha^* = \int \alpha(a') \frac{1 - \sqrt{1 - 4\Theta(a')}}{2\Theta(a')} F(a') da' \,; \tag{6}$$

$$\Theta(a') = \frac{8\pi}{3} N\alpha(a') \int \frac{\alpha(a)}{(a' + a)^3} F(a) da \tag{7}$$

where $\alpha(a)$ is the polarizability of a QD of radius a. For uniform-size QDs Eqs. (6) and (7) reduce

to

$$\alpha^\star(a) = \frac{2a^3}{f\tilde{\alpha}}\left(1-\sqrt{1-f\tilde{\alpha}^2}\right)$$

where $\tilde{\alpha} = \alpha/a^3$. $\alpha^\star$ replaces α in Eq. (4) [notice that for small QD volume fraction f we get $\alpha^\star = \alpha$].

Using the mean-field idea of the absence of scattering "on average" in a composite where its constituents are present in comparable fractions,[26] we can generalize BA by taking into account the QD radius dispersion. Thus, we introduce the modified BA (MBA) for ε^* through the following equation,

$$f\int \frac{\varepsilon_{QD}(a',\omega)-\varepsilon^\star}{\varepsilon_{QD}(a',\omega)+2\varepsilon^*}F(a')da' + (1-f)\frac{\varepsilon_h-\varepsilon^*}{\varepsilon_h+2\varepsilon^*} = 0\,. \tag{8}$$

The case of CdSe spherical QDs

Within the simplest model neglecting the Coulomb interaction between the electron and hole (strong confinement limit) and multiple sub-band structure of the valence band, the QD exciton spectrum is given by[27]

$$E_i = E_g + \frac{\hbar^2\xi_i^2}{2\mu a^2} \tag{9}$$

where E_g is the band gap energy (=1.75 eV for CdSe), μ is the electron-hole reduced mass and $\xi_1 = \pi$, $\xi_2 \approx 4.49$, $\xi_3 \approx 5.76, \ldots$ are the roots of the spherical Bessel functions. Within this model, $\beta_i = 2$ for all $i \geq 1$. [2] The dipole moment matrix element can be expressed as

$$d_{cv} = \frac{e\hbar}{im_0E_g}p_{cv}$$

[2] We use this model for the sake of simplicity. Generalization to the more realistic one[28,29] taking into account the complex valence band structure of the underlying material and the fine structure of the confined hole states is straightforward.

where m_0 is the free electron mass and $2p_{cv}^2/m_0 \approx 20$ eV.[29] We take $\varepsilon_h = 1.5$ for PMMA matrix and assume a Gaussian distribution of the QD radius,

$$F(a) = \frac{1}{\sqrt{2\pi\Delta_a^2}} \exp\left[-\frac{(a-\bar{a})^2}{2\Delta_a^2}\right]$$

where the mean, $\bar{a}$, and the variance, Δ_a, describe QD's average radius and size dispersion, respectively. The real and imaginary parts of the effective dielectric function of the QD/PMMA composite calculated for $f = 0.1$ and 0.3 are shown in Fig. 1. A small imaginary part, $\Gamma = 1$ meV, was introduced in the denominators of Eq. (1).

As it can be seen from Fig. 1, the imaginary part of the effective dielectric function has a resonance at the exciton frequency, with the broadening depending on the QD concentration and size dispersion. The real part of ε^* can reach negative values in the vicinity of the exciton frequency only for vanishing dispersion [Fig. 1(a)], while for larger dispersion it always remains positive [compare with Figs. 1(b) and 1(c)]. For higher f [Fig.1(d)] the difference in the real part of ε^* in the vicinity of the resonance becomes more pronounced. At the same time, increasing the filling factor results in an increase and the proportional broadening of the peaks of the imaginary part of the effective dielectric function [compare Figs. 1(c) and 1(d)]. This is in qualitative agreement with the experimentally measured absorption spectra of dilute dispersions and close-packed films of nanocrystal QDs.[30]

SPP's at metal/NC-layer interface

In order to demonstrate the involved physics, we shall first discuss the dispersion relation for surface plasmon-polaritons[31] in a simplified structure. Let us consider an electromagneic wave in the vicinity of a plane interface between two semi-infinite media, a metal and a QD/dielectric composite, and assume that the wave is $p-$polarized. We choose x axis along the direction of propagation of the electromagnetic wave within the interface plane and z axis perpendicular to the interface. Assuming electromagnetic field's time and x-coordinate dependence to be of the form

$\exp(ikx - i\omega t)$ (where k and ω are the wavenumber and frequency, respectively), we can write down the SPP dispersion relation in the form:[32,33]

$$\frac{\varepsilon_M(\omega)}{p_M} + \frac{\varepsilon^*(\omega)}{p^*} = 0, \tag{10}$$

where $p_M = \sqrt{k^2 - \kappa^2 \varepsilon_M(\omega)}$, $p^* = \sqrt{k^2 - \kappa^2 \varepsilon^*(\omega)}$, $\kappa = \omega/c$ and $\varepsilon_M(\omega)$ is the Drude-type dielectric function of the metal. Eq. (10) can be solved for the wavenumber k, yielding

$$k = \kappa \left(\frac{\varepsilon^*(\omega)\varepsilon_M(\omega)}{\varepsilon^*(\omega) + \varepsilon_M(\omega)} \right)^{1/2}. \tag{11}$$

The amplitude of the electromagnetic wave decays exponentially at both sides of the interface, $\sim \exp(-p^* z)$ for $z > 0$ and $\sim \exp(p_M z)$ for $z < 0$.

The frequency dependence of the real and imaginary parts of k for an Ag/QD–PMMA interface is shown in Figs. 2(a), 2(c), 2(e) and 2(g). $\mathrm{Im}(k)$ increases drastically in the vicinity of QD exciton transition frequencies. It reflects the resonant coupling between SPPs and QD excitons. Again, the resonance peak broadens with the increase of the QD size dispersion [compare Figs.2(a), 2(c), 2(e)] because of the weaker coupling involving fewer QDs for each given ω. Notice that the strengthening and relative narrowing of the resonance peak can be achieved by increasing the filling factor f [compare Figs. 2(e) and 2(g)].

As known, SPPs can be probed in the ATR geometry schematically shown in Fig. 3. The system consists of a prism, an Ag film [3], and a semi-infinite layer of CdSe QD–PMMA composites. Qualitatively the mechanism of SPP's excitation can be expressed in the following manner. The frequency and the x-projection of the wavevector of an external electromagnetic wave, connected by the relation known as "ATR scanline",

$$k_x = \frac{\omega}{c} \sqrt{\varepsilon_g} \sin\theta \tag{12}$$

[3]For the dielectric function of silver we used the expression and parameters given in Ref. [34]

should match ω and $\mathrm{Re}(k)$ of the surface polaritons.[31] In Eq.(12) ε_g is the dielectric constant of the prism and θ is the angle of incidence. In other words, the ATR scanline should intersect the SPP dispersion curve given by Eq.(11) in the case of a single interface. The matching is achieved by adjusting ω and/or θ and is detected by measuring the reflectance, R, which shows characteristic dips corresponding to the resonant transfer of the electromagnetic energy into SPPs.

The reflectivity of the structure depicted in Fig. 3 can be obtained using the transfer matrix formalism (see Supporting Information for details). The SPP properties, qualitatively similar to those outlined above for the simplified structure containing just two semi-infinite media, determine the features of the ATR reflectivity spectra of the system. The minima in the ATR spectra shown in Figs. 2(b), 2(d), 2(f), and 2(h) correspond to the intersections of the SPP dispersion curves with the ATR scanline and resemble the structure of the corresponding $\mathrm{Re}(k)$ *versus* ω dependencies [Figs. 2(a), 2(c), 2(e), and 2(g)].

Results and discussion

Let us consider the properties of the exciton-SPP resonances in more detail. For an arbitrary multi-layer structure, the SPP dispersion relation can also be obtained using the transfer matrix formalism (see Eq. (9) in the Supporting Information). This relation between ω and k may determine multiple branches corresponding to different EM eigenmodes of the structure itself (without ATR prism). If we neglect the imaginary part of the SPP wavevector (damping), the intersections of the $\omega(k)$ curves with the ATR scanline correspond to the resonances. Adding a new layer may result in an additional resonance. Already considering finite QD composite layer requires the full treatment because it may be necessary to take into account the reflection at its interface with vacuum. The calculated results for this case are presented in Fig. 4.

How does the CdSe QD–PMMA layer thickness influence the ATR spectrum? In the case of semi-infinite composite with CdSe NCs [Figs. 2(f)] the resonant interaction of modes occurs at $\theta \approx 50^o$ for $f = 0.1$, $\Delta_a = 0.1\bar{a}$. If the QD–PMMA layer thickness is finite [see the structure

sketch in the inset of Fig. 4(d)], the ATR resonance minima are shifted to lower angles of incidence [compare Figs. 2(f) and 4(a)]. This shift increases with the decrease of the thickness [Fig. 4(d)]. At the same time, the intensity of the SPP-exciton interaction becomes lower. For example, in the case of Fig. 4(d) the resonance is hardly distinguishable (as confirmed also by Fig.4(f), where the positions of resonant minima are shown explicitly).

In the vicinity of the resonant angle ($\theta \approx 42.5^o$ in Fig. 4(b) and $\theta \approx 39^o$ in Fig. 4(e)) the dependence $R(\omega)$ exhibits *two* minima with approximately equal depth, while for other angles of incidence one of the minima is significantly deeper than the other [see Fig. 4(b,e)]. This is characteristic of mode anticrossing and corresponds to the experimental observation of Ref.[21] The positions of these minima (i.e., the angles of incidence, θ_{min}, at which the reflectance reaches its minimum, R_{min}, for a given frequency) are depicted in Fig. 4(c,f), where one can clearly see the resonant SPP-exciton interaction, or mode anticrossing. Thus, with the decrease of the QD–PMMA layer thickness, the mode anticrossing becomes weaker as manifested by the smaller separation of the reflectance minima in Fig. 4(e) for $\theta \approx 39^o$, as well as in Fig. 4(f). The change in the reflectivity spectrum when the angle θ is tuned into resonance, shown in Fig. 4(e), can be compared to the experimental data of Ref.[21] showing a good agreement with Fig. 3 of that article. The depth of the resonant minima of the reflectivity, $R_{min}(\omega)$, at the corresponding angles θ_{min} demonstrates that there are at least three points ($\omega \approx 2.2\,\mathrm{eV}$, $\omega \approx 2.47\,\mathrm{eV}$, $\omega \approx 2.7\,\mathrm{eV}$) where the reflectivity of the ATR structure reaches zero, $R_{min} = 0$. The values of R_{min} far from the exciton resonance frequency are higher for smaller d_1 [compare Figs. 4(c) and 4(f)].

Now let us turn to the structures with the same silver film and *two* composite layers, one of thickness d_1 containing QDs of average radius a_1 and the other (semi-infinite) with QDs of radius a_2 [Fig. 5(a)]. In the ATR spectrum of this structure [Figs. 5(b), 5(e)], one can observe resonances corresponding to both a_1 [$\omega \approx 2.12\,\mathrm{eV}$, $\omega \approx 2.5\,\mathrm{eV}$ and $\omega \approx 2.95\,\mathrm{eV}$] and a_2 QDs [$\omega \approx 2.3\,\mathrm{eV}$ and $\omega \approx 2.85\,\mathrm{eV}$]. Increasing d_1 results in a stronger anticrossing between the SPP and the a_1 QD exciton modes, and in a weakening of the a_2 resonance [compare Figs. 5(b) and 5(e)]. Nevertheless, choosing an appropriate composite layer thickness, one can achieve SPP coupling to

QD excitons localized in the composite layer which is not adjacent to the metallic film.

The ATR minima correspond to some particular values of ω and θ for which the energy of the incident electromagnetic wave is most efficiently transferred to SPP and, consequently, to the QD excitons. This is shown in Figs. 5(c), 5(d), 5(f) and 5(g), where the squared average amplitude of the electric field is plotted for each of the CdSe QD–PMMA layers. It represents the intensity of excitation of QDs located in the layer. If these dots can emit light[4], the relative intensity of light of different colours emitted by two or more composite layers containing QDs of different average radii can be controlled by sdjusting the angle of incidence or the excitation frequency. It may open the possibility of building a lighting device based on a planar structure of multiple NC layers, similar to that presented in Ref.,[13] with controllable color characteristics.

If the average size of the NCs belonging to different layers of the structure is chosen in such a way that the frequencies of the excitonic resonances are different but close to each other, then it is possible to achieve the double resonance (or double anticrossing) due to the simultaneous interaction of SPPs with two kinds of excitons. In this case the ATR spectrum contains *three* minima correspond to one value of θ, as illustrated in the Supporting Information [Figs. S1(a) and S1(b)]. It agrees with the experimental observation of Ref.[35] and corresponds to a SPP-mediated hybridization of slightly detuned excitons.

Finally, we considered several other types of potentially interesting sandwich-type structures containing two or three interfaces between silver and CdSe QD–PMMA composite (see Supporting Information, Fig. S2) and also periodic sequences of metallic and composite layers, i.e. "superlattices" (Fig. 6). For the former, the calculated reflectivity spectra contain (at different θ for a given frequency) two or three minima, respectively, as it might be expected. There is a rather complex "bunching" of modes in the vicinity of the excitonic resonance. The tendency holds for "superlattices" (SLs) of alternating NC composite and metal layers. In order to explain the properties of the ATR structures containing a SL, in Fig. 6(a) we depict the dispersion curves of SPPs in SLs with layer's parameters identical to those of Figs. S2(a, b). The SPP spectrum of an infinite SL can be

[4]The neighborhood of the metallic layer may lead to the quenching of the QD emission.

obtained using the Bloch theorem (see Supporting Information for details of the calculation) and consists of two finite-width bands [shaded regions in Fig. 6(a)] separated by a gap. The edges of the bands correspond to the SPP dispersion curves with Bloch vectors $q_B = 0$ and $q_B = \pi/D$, respectively ($D = d^* + d_M$ is the SL period). Notice that at a certain SPP frequency, $\omega_0 \approx 2.68\,\mathrm{eV}$, the gap in the spectrum disappears. At the same time, the dispersion curve of a finite SL truncated by silver (the dispersion relation is derived in Supporting information) extends to the frequencies $\omega > \omega_0$, while the spectrum of a SL truncated by CdSe QD–PMMA composite exists only for $\omega < \omega_0$. These curves are located inside the gap between the two bands of the SPP spectrum of the infinite SL. Notice that decreasing the silver layer thickness in the SL [see Fig. 6(b)] leads to a broadening of the bands of the SPP spectrum and a red shift of ω_0 [note $\omega_0 \approx 1.82\,\mathrm{eV}$ in Fig. 6(b)]. In the finite SL the spectra corresponding to the infinite SL are quantized (because of the finite number of periods). Not all of the modes are clearly seen in the scale of Figs. 6(c) and 6(d), in fact, the number of the observed minima is less than the number of metal-dielectric interfaces in the structure. However, the surface mode, localized at the metal-SL interface, is clearly seen in Fig. 6(c) at $\omega > \omega_0$. At the same time, in Fig. 6(d) the surface mode is seen both at $\omega > \omega_0$ and $\omega < \omega_0$ (in the frequency range $\omega < \omega_0$ the reflectivity minima correspond to the CdSe QD–PMMA composite/SL interface, the last one truncating the superlattice).

Conclusion

In summary, we have shown that the resonant coupling between the plasmon-polaritons propagating along the metal/NC-layer interface and the excitons confined in chemically synthesized semiconductor NCs, experimentally observed in Ref.,[21] are nicely described theoretically using the appropriate effective dielectric function for the NC composite layer and the standard multilayer optics. The SPP-exciton interaction produces a considerable effect on the optical properties of the structure if the dispersion of the NC size in the composite layer is not too large. In particular, it can be used for obtaining the metal-enhanced fluorescence of QDs.[17] Moreover, we have

shown that combining several composite layers with appropriately sized quantum dots and/or more than one metallic films can result in interesting interactions between the various SPP and exciton modes. Owing to these interactions, the energy of an incident electromagnetic wave can be distributed, by means of surface plasmons, between the different QD species, as it has been suggested for molecules adsorbed on a metallic surface.[36] It can provide the possibility to control the relative intensity of pumping of the QDs of different sizes layer-by-layer assembled into a planar structure. Also, it can lead to the coupling of slightly detuned excitons localized in different layers.[35] In a hypothetical structure containing a (silver/CdSe QD - PMMA composite) superlattice, the coupled SPP-exciton modes are expected to form Bloch bands leading to broad resonances in the ATR spectra. It would be interesting to study this effect experimentally.

Acknowledgement

The work was supported by the FCT (Portugal) under the grant PTDC/FIS/113199/2009.

Supporting Information Available

Supporting Information. Details of the reflectivity and SPP dispersion relation calculations for multilayer structures and superlattices and additional illustrative examples. This material is available free of charge via the Internet at `http://pubs.acs.org/`.

References

(1) Grundmann, M. et al. *Phys. Rev. Lett.* **1995**, *74*, 4043–4046.

(2) Empedocles, S. A.; Norris, D. J.; Bawendi, M. G. *Phys. Rev. Lett.* **1996**, *77*, 3873–3876.

(3) Michler, P. (Ed.) *Single Semiconductor Quantum Dots*; Springer-Verlag: Berlin, 2009.

(4) Kiravittaya, S.; Rastelli, A.; Schmidt, O. G. *Rep. Prog. Phys.* **2009**, *72*, 046502.

(5) Rogach, A. L. (Ed.) *Semiconductor Nanocrystal Quantum Dots*; Springer-Verlag: Wien, 2008.

(6) Crooker, S. A.; Hollingsworth, J. A.; Tretiak, S.; Klimov, V. I. *Phys. Rev. Lett.* **2002**, *89*, 186802.

(7) Caruge, J. M.; Halpert, J. E.; Wood, V.; Bulovic, V.; Bawendi, M. G. *Nature Photonics* **2008**, *2*, 247–250.

(8) Konstantatos, G.; Howard, I.; Fischer, A.; Hoogland, S.; Clifford, J.; Klem, E.; Levina, L.; Sargent, E. H. *Nature* **2008**, *442*, 180–183.

(9) Dyal, S.; Kopidakis, N.; Olson, D. C.; Ginley, D. S.; Rumbles, G. *Nano Lett.* **2010**, *10*, 239–242 .

(10) Balberg, I.; Savir, E.; Dover, Y.; Portillo Moreno, O.; Lozada-Morales, R.; Zelaya-Angel, O. *Phys. Rev. B* **2007**, *75*, 153301.

(11) Döllefeld, H.; Weller, H.; Eychnüller, A. *Nano Lett.* **2001**, *1*, 267–269.

(12) Al-Ahmadi, A. N.; Ulooa, S. E. *Appl. Phys. Lett.* **2006**, *88*, 043110.

(13) Franzl, T.; Klar, T. A.; Scheitinger, S.; Rogach, A. L.; Feldmann, J. *Nano Lett.* **2004**, *4*, 1599–1603.

(14) Santos, J. R.; Vasilevskiy, M. I.; Filonovich, M. I. *Phys. Rev. B* **2008**, *78*, 245422.

(15) Basko, D. M.; Agranovich, V. M.; Bassani, F.; La Rocca, G. C. *Eur. Phys. J. B* **2000**, *13*, 653–659.

(16) Achermann, M.; Petruska, M. A.; Kos, S.; Smith, D. L.; Koleska, D. D.; Klimov, V. I. *Nature* **2004**, *429*, 642–646.

(17) Pompa, P. P.; Martiradonna, L.; Della Torre, A.; Della Sala, F.; Manna, L.; De Vittorio, M.; Calabi, F.; Cingolani R.; Rinaldi, R. *Nature Nanotechnology* **2006**, *1*, 126–130.

(18) Fu, M.; Wang, K.; Long, H.; Yang, G.; Lu, P.; Hetsch, F.; Susha, A. S.; Rogach A. L. *Appl. Phys. Lett.* **2012**, *100*, 063117.

(19) Chen, Z.; Berciaud, S.; Nuckolls, C.; Heinz, T. F.; Brus, L. E. *ACS Nano* **2010**, *4*, 2964–2964.

(20) Rakovich, A. et al., *Nano Lett.* **2010**, *10*, 2640–2648.

(21) Gomez, D. E.; Vernon, K. C.; Mulvaney, P.; Davis, T. J. *Nano Lett.* **2010**, *10*, 274–278.

(22) Maxwell–Garnett, J. C. *Philos. Trans. R. Soc. London* **1904**, *203*, 385–420.

(23) Bruggeman, D. A. G. *Ann. Physik (Leipzig)* **1935**, *24*, 636–679.

(24) Vasilevskiy, M. I.; Anda, E. V. *Phys. Rev. B* **1996**, *54*, 5844–5851.

(25) Vasilevskiy, M. I. *phys. stat. sol. (b)* **2000**, *219*, 197–204.

(26) Landauer, R. In: *Electrical Conductivity In Inhomogeneous Media*, *AIP Proc. V.* **1978**, *40*, 2–45.

(27) Brus, L. E. *J. Chem. Phys.* **1984**, *80*, 4403–4409.

(28) Sercel, P. C.; Vahala, K. J. *Phys. Rev. B* **1990**, *42*, 3690-3710.

(29) (a) Efros, Al. L. *Phys. Rev. B* **1992**, *46*, 7448–7458; (b) Efros, Al. L.; Rosen, M.; Kuno, M.; Nirmal, M.; Norris, D. J.; Bawendi, M. *Phys. Rev. B* **1996**, *54*, 4843–4856.

(30) Leatherdale, C. A.; Bawendi, M. *Phys. Rev. B* **2001**, *63*, 165315.

(31) Pitarke, J. M.; Silkin, V. M.; Chulkov, E. V.; Echenique, P. M. *Rep. Prog. Phys.* **2007**, *70*, 1–87.

(32) Raether, H. *Surface Plasmons on Smooth and Rough Surfaces and on Gratings*; Springer-Verlag: Berlin, 1988.

(33) Cottam, M. G.; Tilley, D. R. *Introduction to Surface and Superlattice Excitations*; Cambridge University Press: Cambridge, 1989.

(34) Johnson, P. B.; Christy, R. W. *Phys. Rev. B* **1972**, *6*, 4370–4379. (1972).

(35) Gomez, D. E.; Vernon, K. C.; Mulvaney, P.; Davis, T. J. *Appl. Phys. Lett.* **2010**, *96*, 073108.

(36) Weiderrecht, G. P.; Hall, J. E.; Boutheiler, A. *Phys. Rev. Lett.* **2007**, *98*, 083001.

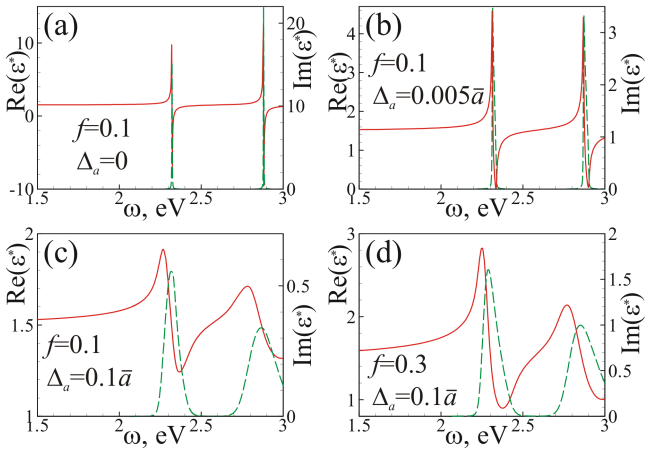

Figure 1: Real (solid lines) and imaginary (dashed lines) parts of the CdSe QD - PMMA composite dielectric function for average QD radius $\bar{a} = 3\,\text{nm}$, calculated using either MMGA with filling factor $f = 0.1$ and QD radius dispersion $\Delta_a = 0$ (panel a), $\Delta_a = 0.005\bar{a}$ (panel b), and $\Delta_a = 0.1\bar{a}$ (panel c), or MBA with filling factor $f = 0.3$ and QD radius dispersion $\Delta_a = 0.1\bar{a}$ (panel d).

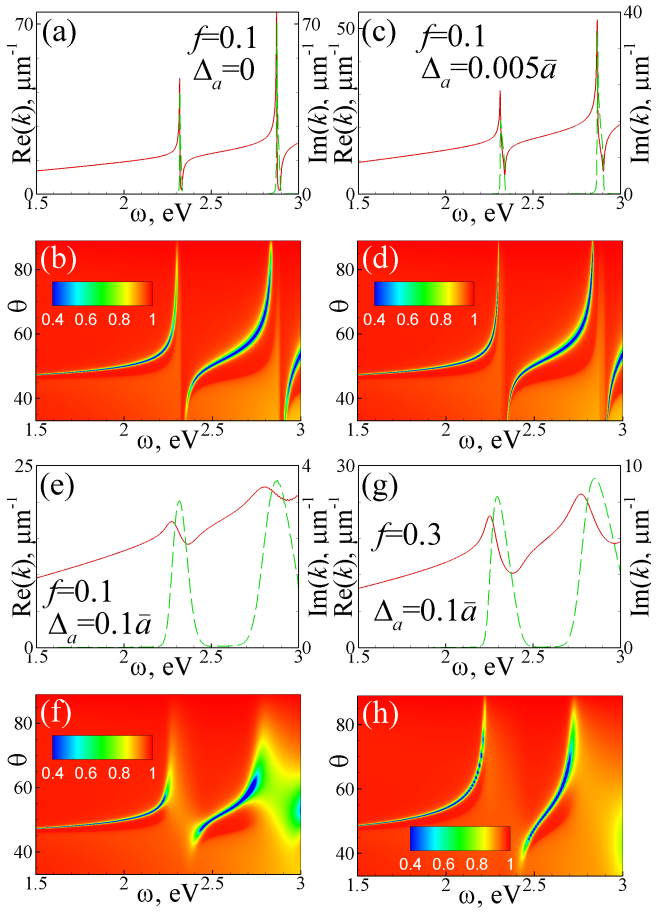

Figure 2: (a, c, e, g) Real (solid lines) and imaginary (dashed lines) parts of the SPP wavevector versus frequency, calculated for the interface between semiinfinite CdSe QD - PMMA composite and silver. (b, d, f, h) Reflectivity R *versus* angle of incidence θ, and frequency ω for the ATR structure with a glass prism ($\varepsilon_g = 2.9584$), a silver film of thickness $d = 53.3$ nm, and a semiinfinite composite medium. The composite dielectric function was calculated for average QD radius $\bar{a} = 3$ nm using MMGA with filling factor $f = 0.1$, and $\Delta_a = 0$ (panels a, b), $\Delta_a = 0.005\bar{a}$ (panels c, d), and $\Delta_a = 0.1\bar{a}$ (panels e, f) or MBA with filling factor $f = 0.3$ and $\Delta_a = 0.1\bar{a}$ (panels g, h).

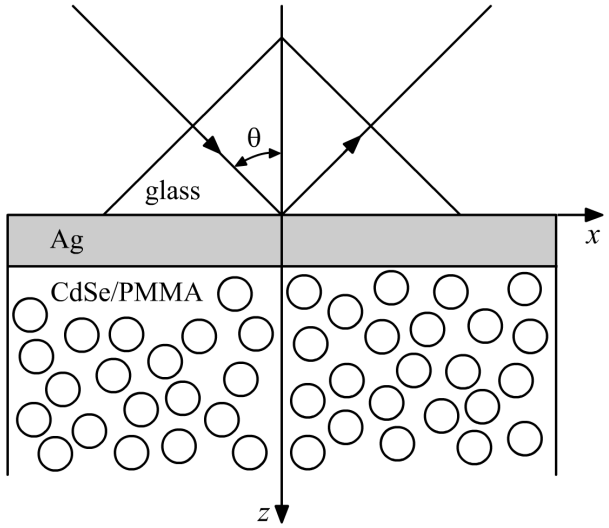

Figure 3: ATR structure composed of a glass prism, a silver plate, and a semi-infinite composite layer containing semiconductor QDs.

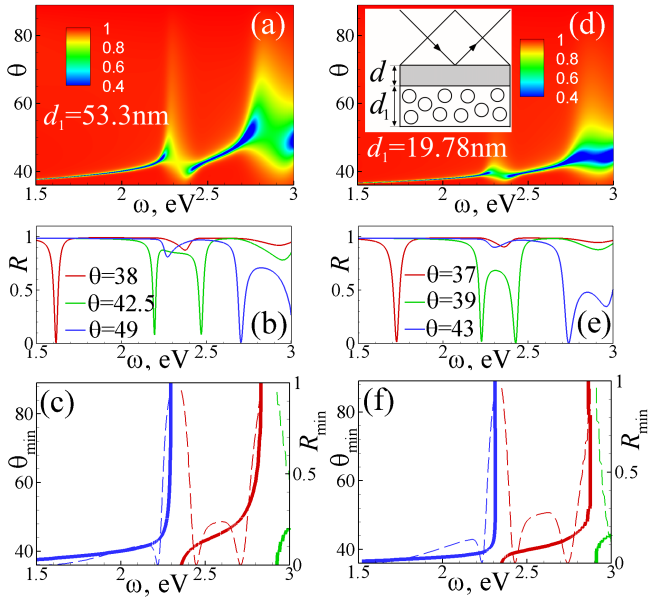

Figure 4: Reflectivity *versus* angle of incidence (θ) and frequency (ω) [panels (a, d)]; reflectivity *versus* frequency ω for a fixed θ [panels **(b, e)**]; minimal reflectivity R_{min} (dashed lines) and corresponding angle of incidence θ_{min} (solid lines) for a given ω [panels **(c, f)**] for the ATR structure [depicted in inset of panel (d)] with glass prism $\varepsilon_g = 2.9584$, silver film of thickness $d = 53.3\,\text{nm}$, CdSe QD–PMMA composite layer of thickness $d_1 = 53.3\,\text{nm}$ (a–c), or $d_1 = 19.78\,\text{nm}$ (d–f), followed by semi-infinite vacuum. The composite dielectric function was calculated using MMGA with $f = 0.1$, $\bar{a} = 3\,\text{nm}$ and $\Delta_a = 0.1\bar{a}$.

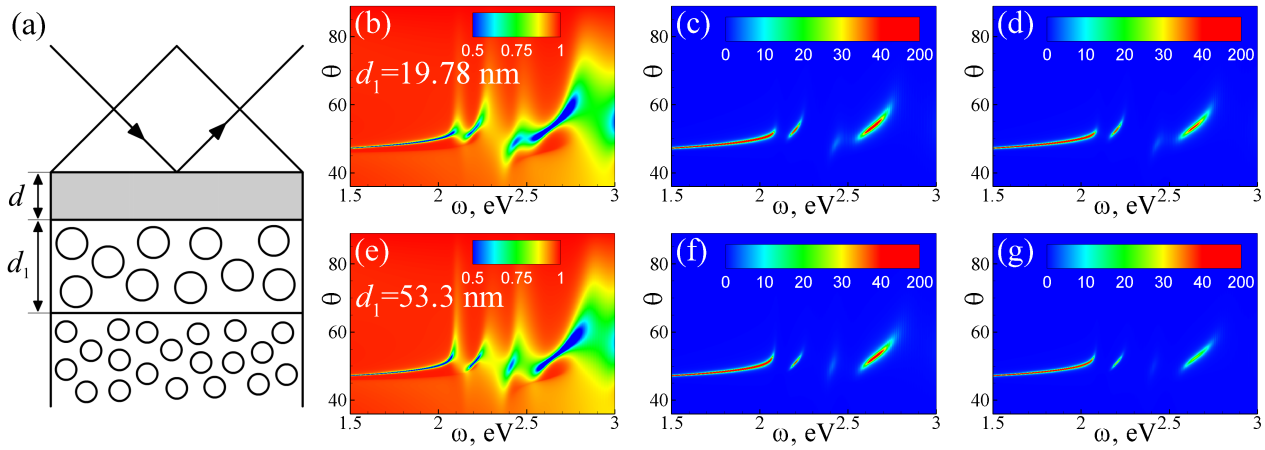

Figure 5: (a) ATR structure consisting of glass prism ε_g, Ag film of thickness d and two CdSe QD–PMMA composite layers, one of thickness d_1, and the other semi-infinite. (b–g) Reflectivity [panels (b, e)], and relative electric field square amplitude $|E_x(z)/E_i|^2$ at $z = d$ [panels (c, f)] and $z = d + d_1$ [panels (d, g)] *versus* angle of incidence and frequency for the structure depicted in panel (a) with $\varepsilon_g = 2.9584$, $d = 53.3\,\text{nm}$, $d_1 = 19.78$ nm (a–c) or $d_1 = 53.3\,\text{nm}$ (d–e). The dielectric functions for both CdSe QD–PMMA composite layers were calculated using MMGA with $f = 0.1$, average QD radii $a_1 = 3.7\,\text{nm}$ (finite layer), $a_2 = 3\,\text{nm}$ (semi-infinite layer), and QD radius dispersions $\Delta_a = 0.1 a_{1,2}$.

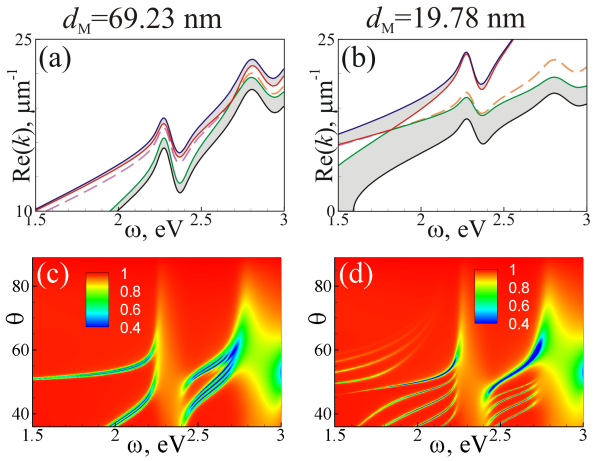

Figure 6: SPP dispersion relations and reflectivity spectra of structures containing a (silver/CdSe QD - PMMA composite) superlattice. Panels (a, b): Real part of the SPP wavevector versus frequency, calculated for a SL with layer thicknesses $d^* = 300\,\text{nm}$ and $d_M = 69.23\,\text{nm}$ (a) or $d_M = 19.78\,\text{nm}$ (b). Shaded regions, bordered by the lines corresponding to the Bloch vectors $q_B = 0$ (green and red solid lines) and $q_B = \pi/D$ (blue and black solid lines) represent two bands of the SPP spectrum in the infinite SL, while the dashed lines correspond to the surface modes of the SLs terminated by a silver (orange lines) or QD–PMMA composite (pink lines) semi-infinite medium; Panels (c, d): Reflectivity *versus* angle of incidence and frequency for the ATR structure consisting of glass prism, one silver film of thickness $d = 53.3\,\text{nm}$, and a 5 period SL of CdSe QD–PMMA composite and Ag terminated by a semi-infinite CdSe QD–PMMA composite medium.

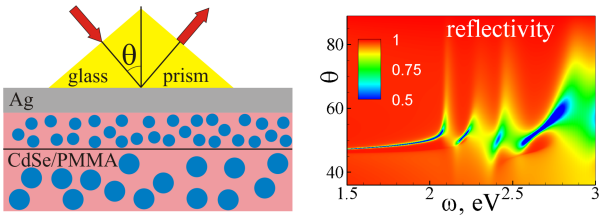

Figure 7: TOC figure